



**HAL**  
open science

## Effect of induced defects on conduction mechanisms of noble-gas-implanted ScN thin films

Razvan Burcea, Hugo Bouteiller, Simon Hurand, Per Eklund, Jean-François Barbot, Arnaud Le Febvrier

► **To cite this version:**

Razvan Burcea, Hugo Bouteiller, Simon Hurand, Per Eklund, Jean-François Barbot, et al.. Effect of induced defects on conduction mechanisms of noble-gas-implanted ScN thin films. *Journal of Applied Physics*, 2023, 134 (5), pp.055107. 10.1063/5.0137428 . hal-04521176

**HAL Id: hal-04521176**

**<https://hal.science/hal-04521176>**

Submitted on 26 Mar 2024

**HAL** is a multi-disciplinary open access archive for the deposit and dissemination of scientific research documents, whether they are published or not. The documents may come from teaching and research institutions in France or abroad, or from public or private research centers.

L'archive ouverte pluridisciplinaire **HAL**, est destinée au dépôt et à la diffusion de documents scientifiques de niveau recherche, publiés ou non, émanant des établissements d'enseignement et de recherche français ou étrangers, des laboratoires publics ou privés.

RESEARCH ARTICLE | AUGUST 03 2023

# Effect of induced defects on conduction mechanisms of noble-gas-implanted ScN thin films

Razvan Burcea ; Hugo Bouteiller ; Simon Hurand ; Per Eklund ; Jean-François Barbot  ; Arnaud le Febvrier  

 Check for updates

*J. Appl. Phys.* 134, 055107 (2023)

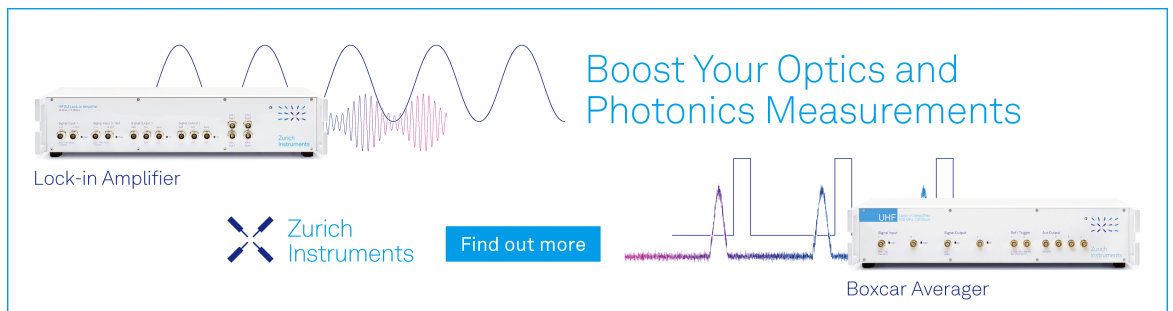
<https://doi.org/10.1063/5.0137428>



View Online



Export Citation



Boost Your Optics and Photonics Measurements

Lock-in Amplifier

 Zurich Instruments

[Find out more](#)

Boxcar Averager

# Effect of induced defects on conduction mechanisms of noble-gas-implanted ScN thin films

Cite as: J. Appl. Phys. **134**, 055107 (2023); doi: [10.1063/5.0137428](https://doi.org/10.1063/5.0137428)

Submitted: 15 June 2023 · Accepted: 15 July 2023 ·

Published Online: 3 August 2023



Razvan Burcea,<sup>1</sup> Hugo Bouteiller,<sup>1</sup> Simon Hurand,<sup>1</sup> Per Eklund,<sup>2</sup> Jean-François Barbot,<sup>1,a)</sup> and Arnaud le Febvrier<sup>2,a)</sup>

## AFFILIATIONS

<sup>1</sup>Institute PPRIME, CNRS, Université de Poitiers—ENSMA, UPR 3346, SP2MI, TSA 41123, 86073 Poitiers Cedex 9, France

<sup>2</sup>Department of Physics, Chemistry and Biology (IFM), Linköping University, SE-581 83 Linköping, Sweden

<sup>a)</sup>Authors to whom correspondence should be addressed: [jean.francois.barbot@univ-poitiers.fr](mailto:jean.francois.barbot@univ-poitiers.fr) and [arnaud.le.febvrier@liu.se](mailto:arnaud.le.febvrier@liu.se)

## ABSTRACT

Noble-gas implantation was used to introduce defects in n-type degenerate ScN thin films to tailor their transport properties. The electrical resistivity increased significantly with the damage levels created, while the electron mobility decreased regardless of the nature of the ion implanted and their doses. However, the transport property characterizations showed that two types of defects were formed during implantation, named point-like and complex-like defects depending on their temperature stability. The point-like defects changed the electrical conduction mode from metallic-like to semiconducting behavior. In the low temperature range, where both groups of defects were present, the dominant operative conduction mechanism was the variable range hopping conduction mode. Beyond a temperature of about 400 K, the point-like defects started to recover with an activation energy of 90 meV resulting in a decrease in resistivity, independent of the incident ion. The complex-like defects were, therefore, the only remaining group of defects after annealing above 700 K. These latter, thermally stable at least up to 750 K, introduced deep acceptor levels in the bandgap resulting in an increase in the electrical resistivity with higher carrier scattering while keeping the metallic-like behavior of the sample. The generation of both types of defects, as determined by resistivity measurements, appeared to occur through a similar mechanism within a single collision cascade.

© 2023 Author(s). All article content, except where otherwise noted, is licensed under a Creative Commons Attribution (CC BY) license (<http://creativecommons.org/licenses/by/4.0/>). <https://doi.org/10.1063/5.0137428>

## I. INTRODUCTION

Ion beam technology is of interest in various areas of materials science and engineering. In particular, the ion implantation technique is used for selective carrier control (doping) in semiconductors. However, the interactions between the incident ion and the target atoms generate high concentrations of point defects, which can develop into different forms depending on the implantation conditions. The as-produced defects or disorders can change the physical material properties and, thus, be favorable or detrimental depending on the applications sought. Determining the correlation between the irradiation-induced defects and the physical properties of materials is, therefore, an important topic along with fundamental studies of defects.

Rock salt structured scandium nitride (ScN) is a narrow indirect bandgap semiconductor that has attracted attention for many

applications in different domains.<sup>1,2</sup> ScN also interests the scientific community studying thermoelectric (TE) materials as it exhibits a large power factor of  $2\text{--}4 \times 10^{-3} \text{ W m}^{-1} \text{ K}^{-2}$  at 800 K.<sup>3–5</sup> However, the main disadvantage of ScN for TE applications is its relatively high thermal conductivity in the range of  $10\text{--}20 \text{ W m}^{-1} \text{ K}^{-1}$  at room temperature (RT).<sup>4,6–10</sup> Calculations have shown that the introduction of defects could improve its thermoelectric properties.<sup>11</sup> Ion implantation has proven to reduce the thermal conductivity and improve the TE figure of merit of ScN films.<sup>12–14</sup> In all cases, the implanted ScN samples exhibited a reduced thermal conductivity, highlighting the role of irradiation-induced defects in phonon scattering. However, depending on the nature of the incident ion, few differences were observed. Rao *et al.* reported that post-implant annealing did not change the thermoelectric properties of Li<sup>+</sup> implanted samples, even though ScN restores its initial

26 March 2024 08:54:35

color. Burcea *et al.* reported a partial recovery of the thermoelectrical properties with a recovery of the color of the film after annealing on Ar-implanted samples.<sup>12,13</sup> The use of implantation techniques to optimize the physical properties of ScN films for specific applications arises the importance of controlling the introduced defects and understanding their evolution upon annealing.

The present study aims to understand the role of defects induced by ion implantation on the electrical conductivity behavior of degenerate ScN thin films. Controlling electrical conductivity is crucial in achieving high power factors and must be closely monitored. This work also extends our previous investigations, on Ar-implanted ScN,<sup>14</sup> by using two noble gases (Ar and He) with their different capabilities to defect formation. The effects of as-introduced defects on the electrical properties and the conduction mode have been investigated in detail, and the damage build-up has been studied through resistivity measurements.

## II. EXPERIMENTAL DETAILS

Epitaxial-like thin films of n-type ScN were deposited using dc reactive magnetron sputtering in an ultrahigh-vacuum chamber onto Al<sub>2</sub>O<sub>3</sub> (c-cut) substrates maintained at 800 °C. More details can be found in a previous work,<sup>12</sup> and the deposition system is described in detail elsewhere.<sup>15</sup> The ScN films show a high electron concentration of about 10<sup>21</sup> cm<sup>-3</sup> due to the presence of unwanted impurities such as oxygen incorporated during deposition.

The 240 nm thick films were ion implanted at room temperature (RT) using the implanter EATON VN3206. The depth profiles of the implanted ions in the ScN films (density of 4.29 g cm<sup>-3</sup>) were calculated using SRIM 2013 software under the full-damage cascade.<sup>16</sup> A multi-energy implantation protocol was used to introduce a constant quantity of damage (called displacements per atom, noted dpa) along the film thickness. The level of dpa, in the range 0.8–6 dpa, was controlled by the fluences of incident ions. As an example, in Fig. 1 is presented the energy profile extracted

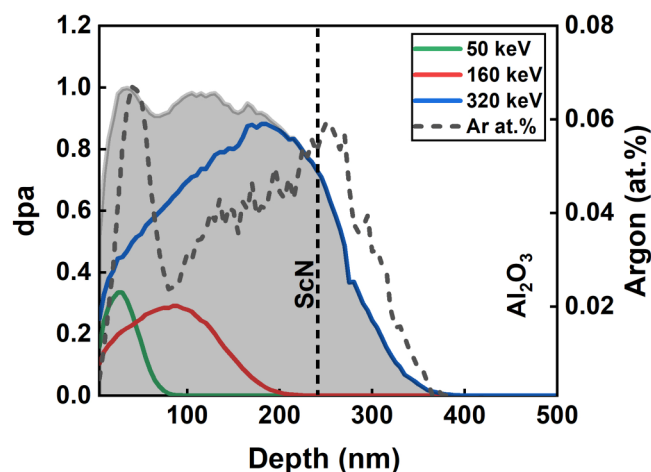


FIG. 1. Displacement per atom (dpa) and concentration profiles as a function of depth calculated using SRIM code for a multi-energy Ar-1dpa implantation.

from SRIM 2013 for a damage level of 1 dpa with argon ions, using three decreasing incident energies of 320, 160, and 50 keV with fluences of  $7 \times 10^{14}$ ,  $2 \times 10^{14}$ , and  $2 \times 10^{14}$  ions cm<sup>-2</sup>, respectively. With these fluences, the concentration of argon atoms introduced fluctuates around 0.05 at. %.

In this study, two different noble gases, helium and argon, were used. With their chemical effects being minimized, their difference in mass yields different ratios of as-created vacancies (V) per incident ion ( $V/\text{Ar}^+ \gg V/\text{He}^+$ ). Therefore, when irradiating with argon ions, dense collision cascades are generated, while when irradiated with helium, only diluted cascades are generated. All the experiments were conducted on the same set of samples to avoid any effect of native impurities on the defect trapping or stability.

Two procedures were used for implantation, the created displacement dose (dpa) was delivered either in one shot (single implantation) or in multiple shots (named cumulative in the following). To clarify the reading, in this paper, three samples were labeled as follows.

§ First sample labeled “Ar-1dpa” was implanted at 1 dpa ( $\sim 0.05$  at. %) with argon using three different energies (Fig. 1). The same sample was then cumulatively implanted at RT. First, it was implanted up to 3 dpa, labeled “Ar-3dpa-cumul,” by adding 2 dpa. Then, the same sample was implanted using 1 dpa step process up to a total of 6 dpa, labeled “Ar-6dpa-cumul.”

§ Second sample labeled “He-0.8 dpa” was implanted at 0.8 dpa ( $\sim 1$  at. %) with a single implantation. The process involved five energies 60, 45, 35, 20, and 10 keV with fluences of  $1 \times 10^{16}$ ,  $1 \times 10^{15}$ ,  $6 \times 10^{15}$ ,  $5 \times 10^{15}$ , and  $3 \times 10^{15}$  ions cm<sup>-2</sup>, respectively.

§ 3rd sample labeled “Ar-cumul” was implanted cumulatively up to 5 dpa with 1 dpa step. For each step, the implantation process was the same as the 1 dpa implantation with argon ions described in Fig. 1.

The macroscopic in-plane resistivity  $\rho(T)$  and mobility  $\mu(T)$  were measured using the van der Pauw method coupled with the Hall effect (ECOPIA HMS-5500). Two measurement setups were used: a low temperature cryostat, from 80 to 350 K, and a high temperature setup, from 300 to 750 K. The temperature increasing rate was about 3 °C min<sup>-1</sup>. Hall measurements were performed using a constant magnetic field of 0.580 T.

## III. RESULTS AND DISCUSSION

Figure 2 shows the  $\rho(T)$  and  $\mu(T)$  data obtained for the as-grown film (reference) and after the argon implantation of 1 dpa at RT (Ar-1dpa). With increasing temperature, the reference  $\rho(T)$  curve is approximately constant in the range 80–150 K. Above 150 K, the resistivity increases linearly with temperature, which is a typical trend of a metallic-like behavior for degenerate semiconductors ( $\bar{n}_e = 2.1 \pm 0.2 \times 10^{21}$  cm<sup>-3</sup>). After Ar-1dpa implantation ( $\Delta$  meas. 1), the resistivity was significantly higher, and the mobility was strongly reduced. The electrical resistivity of the implanted sample decreased continuously, while the electron mobility increased when the temperature was increased. However, the

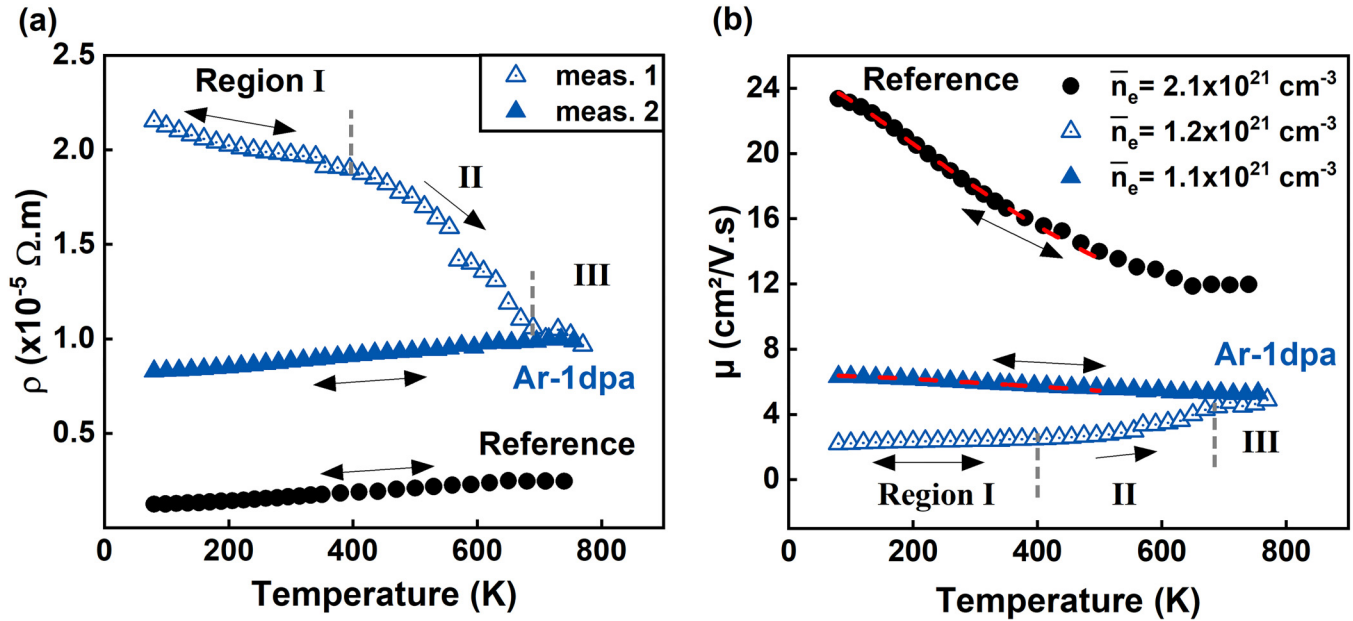


FIG. 2. (a)  $\rho(T)$  of the reference ScN (•) and implanted Ar-1dpa. First ( $\Delta$ ) and second ( $\blacktriangle$ ) measurement are consecutive ( $\leftrightarrow$  reversible behavior,  $\rightarrow$  non-reversible behavior measurement). (b) The corresponding  $\mu(T)$  curves. The red dashed curves are fitted according to the Matthiessen law up to 500 K. All experimental data points were measured on increasing temperature.

density of charge carriers remains relatively constant throughout the entire temperature range, albeit with a lower average value, indicating trapping of charge carriers. This implies modifications of the electrical transport property in ScN.

The  $\rho(T)$  and  $\mu(T)$  curves [Figs. 2(a) and 2(b)] could be divided into three distinct regions. At low temperature from 80 to 400 K (region I), both  $\rho(T)$  and  $\mu(T)$  curves were fully reversible (illustrated by  $\leftrightarrow$ ) where the measurements were repeatable several times. In region II (400–700 K), both measurements [ $\rho(T)$  and  $\mu(T)$ ] were no longer reversible ( $\rightarrow$ ), suggesting the activation of another carrier transport mechanism. The feature, taking place in region II, can be related to an irreversible recombination or recovery of some implantation-induced defects leading to a decrease in resistivity and an increase in mobility with temperature. The recovery process appeared to end at a minimum annealing temperature of around 700 K (region 3). Once this temperature reached, all defects that could *in situ* recombine were removed, and the reversible metal-like degenerate semiconductor behavior of ScN was recovered. This observation was confirmed by the second measurement ( $\blacktriangle$  meas. 2) performed on the same sample for which the metallic-like behavior was fully restored and reversible.

Finally, as for  $T > T_0 = 180$  K, the resistivity ( $\blacktriangle$  meas. 2) can be described by the following equation:

$$\rho(T) = \rho_R + \alpha(T - T_0) + \rho_D, \quad (1)$$

with  $\alpha$  being the slope,  $\rho_R$  the residual resistivity, and  $\rho_D$  the additional resistivity induced by the implantation process. The mobility, on the other hand, can be described according to the Matthiessen

law,

$$\frac{1}{\mu(T)} = \frac{1}{\mu_{lat}(T)} + \frac{1}{\mu_R} + \frac{1}{\mu_D}, \quad (2)$$

with  $\mu_{lat} \sim T^{-1.5}$  being the lattice mobility,  $\mu_R$  the residual mobility, and  $\mu_D$  the additional mobility induced by implantation. On a n-type ScN grown by magnetron sputtering on the MgO substrate, the temperature dependent mobility data were fitted with  $\mu_{lat} \sim T^{-1.3}$ .<sup>17</sup> In the present study, the  $\mu(T)$  curve for the reference sample could not be fitted by considering only lattice mobility and was fitted according to the Matthiessen law [Eq. (2)] up to 500 K, yielding a residual mobility value of  $\mu_R \sim 25 \text{ cm}^2 \text{ V}^{-1} \text{ s}^{-1}$ . Beyond that temperature, the fitted curve starts to deviate suggesting further contributions that have not been considered in the present case. For the Ar-1dpa (meas. 2), the analysis led to an additional term in the mobility,  $\mu_D \sim 9 \text{ cm}^2 \text{ V}^{-1} \text{ s}^{-1}$ , while  $\mu_R$  and  $\mu_{lat}(T)$  were kept unchanged. Concerning the resistivity, the additional term was estimated to be  $\rho_D = 7.16 \times 10^{-6} \Omega \cdot m$ . Both terms ( $\mu_D$  and  $\rho_D$ ) are temperature independent and were attributed to “thermally stable” implanted defects.

After the initial ion implantation, the charge carrier density decreased from approximately  $2.1 \times 10^{21}$  to  $1.1 \times 10^{21} \text{ cm}^{-3}$ . This effect was previously observed with Ar<sup>+</sup> at 5 dpa and ascribed to complex defects acting as traps for free carriers.<sup>14</sup> During annealing, the average carrier concentrations ( $\bar{n}_e$ ) remained roughly constant in the investigated temperature range [Fig. 2(b)]. In the case of Ar-1dpa implantation, no significant differences in  $\bar{n}_e$  between the first

( $\bar{n}_e = 1.2 \pm 0.2 \times 10^{21} \text{ cm}^{-3}$ ) and second measurement ( $\bar{n}_e = 1.1 \pm 0.2 \times 10^{21} \text{ cm}^{-3}$ ) were observed. This observation confirmed that the metastable defects, which recombined *in situ* annealing, did not introduce any deep acceptor levels in the bandgap. However, these metastable defects affected the electronic transport mode. All implanted samples, with either helium or argon ions, exhibited the same behavior after implantation with a change of the conduction mode at low temperature followed by a partial recombination of the defects from 400 K and above.

Regarding the implantation at 1 dpa (Ar-1dpa), two types of defects were generated: (i) complexes of defects, stable at least up to 750 K, affecting the electrical properties of the film by carriers' trapping (creation of deep acceptors levels) and scattering and (ii) implanted-induced defects recombining under *in situ* annealing from 400 K and onwards. These implanted-induced defects were seen as point-like defects and act as carrier scattering and not as traps (no reduction of the carrier concentration). In the case of  $\text{Mg}^+$  implantation at a similar damage dose in ScN thin films, a decrease in  $\rho(T)$  was also observed, suggesting a recombination of defects during the measurement.<sup>12</sup> However, as the measurement was not repeated, it is not possible to confirm whether the defects remained after recombination as is the case for  $\text{Ar}^+$  implantation.

Introduced in large quantity, the point-like defects impact the electrical conduction mode in the low temperature region (I). The negative temperature coefficient of the resistivity implies a semiconductor-like behavior described by

$$\rho(T) = \rho_0 \exp \left[ \left( \frac{E_t}{k_B T} \right)^p \right], \quad (3)$$

where  $\rho_0$  is the resistivity coefficient,  $E_t$  the transition energy, and  $p$  a characteristic component ( $p > 0$ ) defining the mode of electrical conduction.<sup>18</sup> For a transport caused by thermal activation of electrons into the band conduction,  $p = 1$ , while for a transport governed by electron hopping between localized states,  $p$  lies between 0 and 1.

Figure 3 displays the dependence of  $\ln(\rho)$  as a function of  $T^{-1/4}$  [(a) and (b)] and  $T^{-1}$  (c). Figure 3(a) presents a comparison of the plot of  $\ln(\rho)$  vs  $T^{-1/4}$  for the sample Ar-1dpa and the cumulative implanted films Ar-3dpa-cumul and Ar-6dpa-cumul.

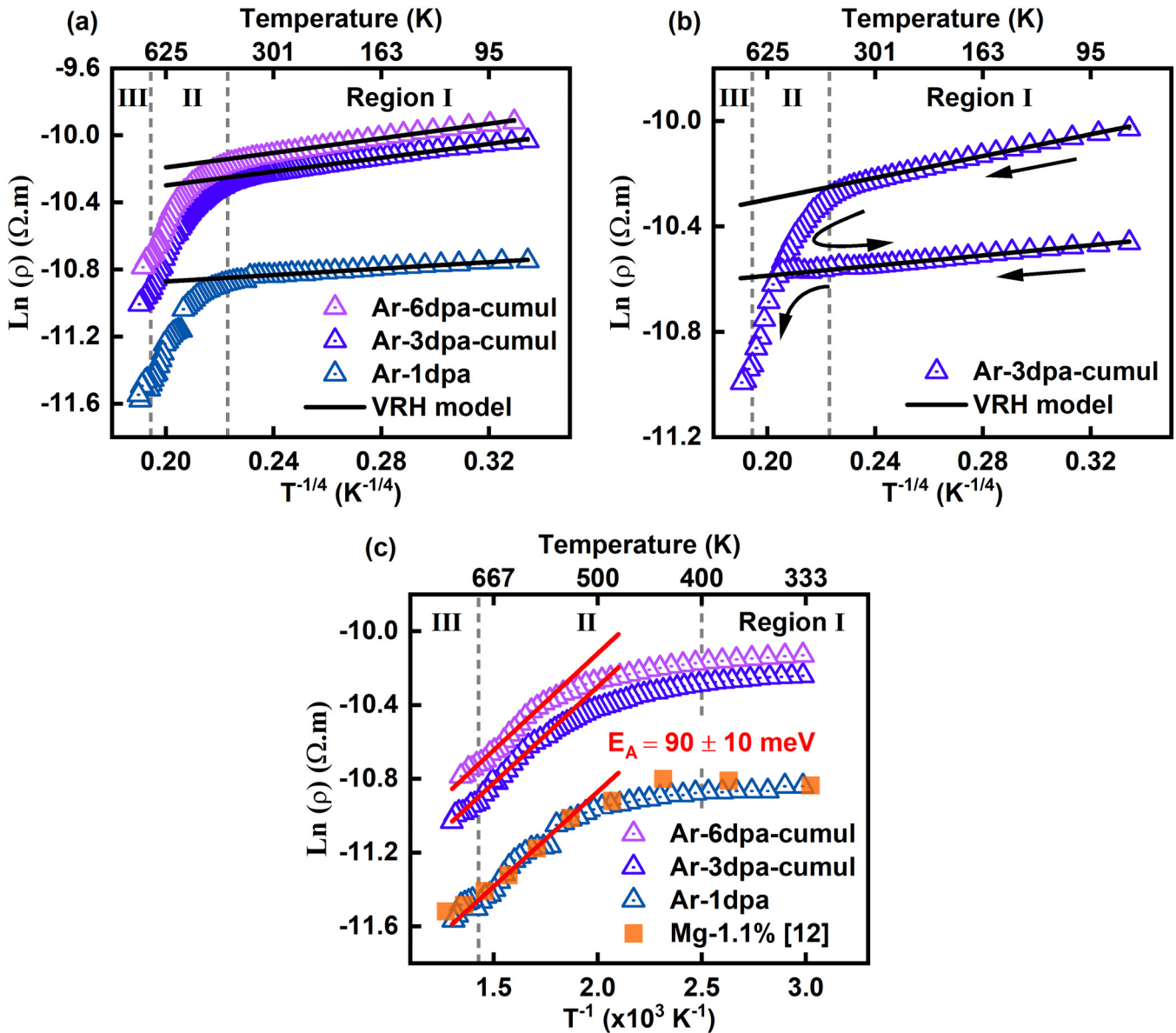
All three  $\ln(\rho)$  vs  $T^{-1/4}$  curves express a similar behavior, i.e., a linear region from 80 to 280 K related to the mechanism of electrical conduction mode, and a change of slope around 400 K marking the beginning of the recombination process. At low temperature ( $T < 400$  K, region I), the band conduction mode, which predicts an Arrhenius dependence of the resistivity, was not valid [ $p = 1$  in Eq. (3)], indicating a different conduction mechanism. However,  $\ln(\rho)$  can be adequately fitted with Eq. (3) and component value of  $p = \frac{1}{4}$ , suggesting a 3D variable range hopping (VRH) conduction mechanism proposed by Mott and Davis.<sup>19</sup> All three  $\ln(\rho)$  vs  $T^{-1/4}$  curves were successfully fitted in region I according to Eq. (3) using  $p = \frac{1}{4}$ . Therefore, it can be stated that the point-like defects yielded localized states around the Fermi level which were responsible for the change of conduction mode with a VRH conduction mechanism in the low temperature region.

For  $T > 400$  K, the recovery of these point-like defects occurred and  $\rho(T)$  and  $\mu(T)$  measurements were not reversible. The VRH

conduction mechanism prevailed at low temperature on all implanted ScN samples with a damage level ranging from 1 to 6 dpa. However, the Mott temperature  $T_M = \frac{E_t}{k_B}$  [slope estimated from Eq. (3) with  $p = \frac{1}{4}$ ] differs between the Ar-1dpa, the Ar-3dpa-cumul, and Ar-6dpa-cumul. For Ar-1dpa,  $T_M$  was equal to 1 K, while for Ar-3dpa,  $T_M$  increased to 16 K and remained unchanged for further argon doses (Ar-6dpa) due to the saturation of electrically active defects as suggested by the cumulative resistivity (Fig. 5). According to Mott's model, this suggested a decrease in the localization parameter  $L_c = D(E_F)\gamma^{-3}$ , where  $1/\gamma$  is the decay length and  $D(E_F)$  the density of states at the Fermi level  $E_F$ . In addition, Kerdsonpanya *et al.* reported that the introduction of vacancies or other defects (impurities or dopants) can modify the DOS by introducing asymmetric peaks or shift the Fermi level in the electronic band.<sup>11</sup> In the present study, defects introduced by noble gas implantation influence both the DOS and the decay length.

Figure 3(b) displays the  $\ln(\rho)$  vs  $T^{-1/4}$  data obtained for Ar-3dpa-cumul. In this case, the measurement was stopped at 600 K and ran again from low temperature to 750 K (see arrows). The resistivity values of the second measurement are lower than the initial measurement until reaching the initial stopping point at 600 K. Beyond 600 K, the resistivity continues to decrease until  $\rho(T)$  and  $\mu(T)$  stabilize. Once again, the low temperature region was fitted according to Mott's equation [Eq. (3)] showing different Mott temperatures between the first and second runs with values of 16 and 1 K, respectively. When the resistivity measurement was interrupted in region II, the partial recombination of point-like defects increased the spatial extension of the localized states. The VRH conduction mode was still prevailing since  $\ln(\rho) \propto T^{-1/4}$  but with a lower  $T_M$ , hence increasing the localization parameter  $L_c$ . It is important to highlight that despite the occurrence of partial recombination of point-like defects when the temperature slightly exceeds 400 K ( $T < 700$  K), the conduction mechanism of variable range hopping (VRH) persists within region I. The only variable in the description of the conduction mechanism is the Mott temperature  $T_M$ . This confirmed that defects' concentration was directly linked to the change of Mott temperature.

Figure 3(c) represents the plot of  $\ln(\rho)$  vs  $T^{-1}$  for Ar-1dpa, Ar-3dpa-cumul, and Ar-6dpa-cumul and compared to the data obtained from  $\text{Mg}^+$  implanted sample previously reported in the literature.<sup>12</sup> In region II, where the number of point-like defects decreases due to their recombination, the resistivity variations follow an Arrhenius law, through linear dependence of  $\ln(\rho)$  vs  $T^{-1}$  curves, with an activation energy value of  $E_A = 90 \pm 10$  meV. Furthermore, the activation process remained independent of the fluence (dpa) or the incident ions ( $\text{Ar}^+$  and  $\text{He}^+$ ) used. The  $\text{Mg}^+$ -implanted sample had a similar activation energy ( $E_A \approx 90$  meV). This comparison showed that the point-like defects involved in recombination originated mostly from ballistic effects rather than the nature of the implanted species. In the case of  $\text{Li}^+$ -implanted n-type ScN/MgO ( $n \sim 10^{20} \text{ cm}^{-3}$ ) at low dose, the increase in resistivity and a decrease in mobility were observed as the dose increased.<sup>13</sup> However, no change in the conduction mechanism and recombination process was reported between 400 and 1000 K. This may suggest that the level of damage (or dose) was a major factor in the production of unstable defects in ScN, unless other factors are relevant to the stability of defects, such as the initial state of the material.



26 March 2024 08:54:35

**FIG. 3.** (a) Plot of  $\ln(\rho)$  vs  $T^{-1/4}$  for the Ar-1dpa thin film and then implanted cumulatively up to 3 and 6 dpa. In the temperature range 80–400 K (region I),  $\ln(\rho)$  vs  $T^{-1/4}$  curves were fitted by the VRH conduction model. (b) Plot of  $\ln(\rho)$  vs  $T^{-1/4}$  for the cumulative Ar-3dpa with an interruption at 600 K followed by a second run (see the arrows). The VRH slopes are clearly different showing a decrease in the Mott temperature when returning to 600 K. (c) Plot of  $\ln(\rho)$  vs  $T^{-1}$  to determine the activation energy of the recovery process in region II (400–700 K: region II) on the increase in temperature. Orange square plot: data obtained on the Mg-implanted ScN case in Ref. 12.

Finally, in region III, once the point-like defects are recombined, only the complex-like defects remained, resulting in (i) a metallic-like behavior similar to pristine sample, (ii) a reduction in the number of carriers via trapping, and (iii) an additional scattering of the carriers. Similarly observed in a previous work on argon implanted ScN, this type of defect generation leads additionally to an increase in the Seebeck coefficient and phonon scattering.<sup>14</sup> The complex-like

defects introduce deep acceptor levels in the bandgap, resulting in an alteration of the color of the samples into non-transparent material.<sup>12–14</sup> In ScN implanted with noble gas, these defects recover or evolve into nanocavities when annealed at high temperatures, causing the implanted ScN to return to its initial color.<sup>14</sup>

Figure 4 displays the  $\rho(T)$  curves obtained after *in situ* annealing (as meas. 2 in Fig. 1) of the samples implanted at RT with two

different regimes of defects generation (0.8 and 1 dpa) using either He or Ar ions and compared to argon implantation at 5 dpa from a previous study.<sup>14</sup> To obtain the same level of damage of 1 dpa created with Ar ions (0.05 at. %), the quantity of He ions injected was about 1 at. %, which was 20 times larger than the concentration of Ar ions. After *in situ* annealing, all samples exhibit the same behavior as the reference sample, namely, a metallic-like behavior. The slope of all  $\rho(T)$  curves is roughly similar  $\alpha = 2.7 \times 10^{-9} \pm 0.4 \times 10^{-9} \Omega \text{ m K}^{-1}$ . Thus, after recombination, only the complex defects remained and only the term  $\rho_D$ , from Eq. (1), was modified:  $\rho_D^{\text{He-0.8dpa}} = 6.1 \times 10^{-6} \Omega \text{ m}$ ,  $\rho_D^{\text{Ar-1dpa}} = 7.1 \times 10^{-6} \Omega \text{ m}$  and  $\rho_D^{\text{Ar-5dpa}} = 1.2 \times 10^{-5} \Omega \text{ m}$ . Therefore, it can be stated that the variation of electrical behavior seemed to be dominant and dependent on the damage level implanted regardless of the nature of implanted ions and their concentration.

The structure of the displacement cascades and, hence, the deposited energy did not seem to affect the formation of primary defects in ScN. However, the values of  $\rho_D$  are much higher than those estimated in the case of  $\text{Mg}^+$  implantation for an equivalent dose, suggesting that the implanted gas promoted their generation by acting as stabilizers. Indeed, the trapping of noble gases by vacancies to form complexes or clusters ( $\text{NG}_n\text{-V}_m$ ,  $m > n$ ) is known to be energetically favorable in semiconductors.<sup>20</sup> These kinds of complexes were suggested to be precursors to form nanocavities under subsequent annealing.<sup>21</sup> If this mechanism is operating in ScN, as previously suggested in Ar-implanted ScN<sup>14</sup> where cavities were observed, then the amount of helium trapped by complex defects should be far greater than argon.

The term complex defects is generic and can refer to various defects such as voids (empty cavities resulting from the

agglomeration of vacancies), bubbles (gas-filled cavities), and even interstitial clusters (that appear as black-spot damage in transmission electron microscopy).<sup>14</sup> In addition, regardless of the damage regime or the ion used, the remaining complex defects did not modify the slopes of the  $\rho(T)$  curves revealing that the electron-phonon scattering was not affected. To show that the electrical conducting behavior at a given temperature in region II does not depend on any kinetic effect of the defect evolution during *in situ* measurement but rather on thermodynamic equilibrium of the defect arrangement, an additional experiment was carried out. A thin film was implanted at 0.9 dpa with He, followed by annealing at 700 K during 10 min in a lamp furnace under dynamic vacuum. As expected, this sample showed a metallic-like electrical behavior with a slope identical to those observed in Fig. 4, demonstrating that the temperature is the key parameter concerning the point-like defect recovery.

Electrical resistivity is sensitive to defects and, therefore, should be an indication of damage accumulation in implanted samples. To understand how the cumulative implantation influences defects formation, a unique sample labeled Ar-cumul was implanted up to 5 dpa in 1 dpa step.

Figure 5 presents the relative change in resistivity at 300 K attributed to either point-like defects or complex-like defects, normalized by the maximum resistivity observed after implantation. The evolutions of both types of defects' contributions on the relative resistivity were compared. The contribution of the point-like defects is given by the difference between meas. 1 and meas. 2, i.e.,  $\Delta\rho_{PD}^{300K} = \rho_{meas.1} - \rho_{meas.2}$  (see Fig. 2). On the other hand, the contribution of the complex-like defects is given by the difference between meas. 2 and the data of the reference measurement, i.e.,  $\Delta\rho_{Complex}^{300K} = \rho_{meas.2} - \rho_{ref}$ . Both defect contributions were compared to a simulation of the disorder accumulation. This simulated model

26 March 2024 08:54:35

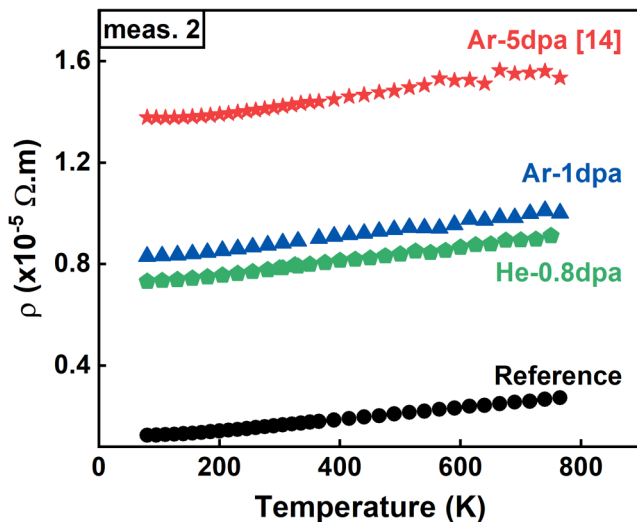


FIG. 4. Resistivity measurements of ScN thin films for reference and after noble-gas implantation under different conditions (meas. 2, i.e., recorded after a first measurement up to 750 K resulting in the *in situ* recovery of one type of defect).

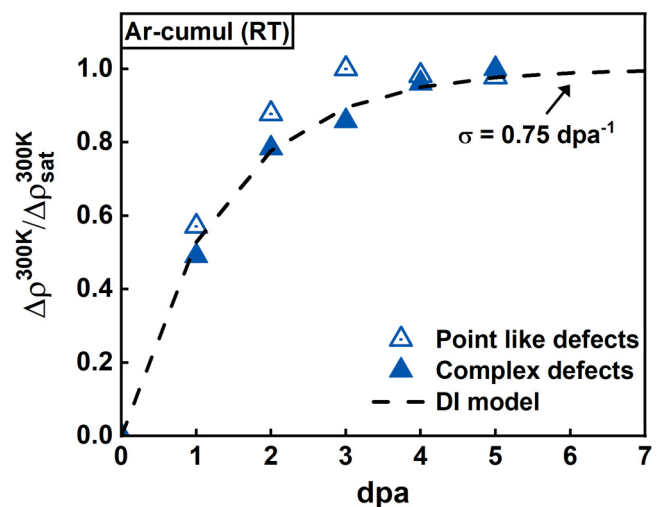


FIG. 5. Plots of the values of relative increase in resistivity, at 300 K, against dose (dpa) for ScN under cumulative argon implantation at RT. The dotted lines represent the direct impact (DI) model described by Eq. (4).

(dashed curve in Fig. 5) was characteristic of a single-hit process (or called the direct impact model) for the creation of defects and could be described by Eq. (4), proposed by Gibbons,<sup>22</sup> which assumes that no cascade recovery is necessary to create a defect,

$$\Delta\rho^{300K} = \Delta\rho_{sat}^{300K}(1 - e^{(-\sigma\phi)}), \quad (4)$$

where  $\Delta\rho_{sat}^{300K}$  is the residual induced defects resistivity level at saturation,  $\sigma$  the cross section for damage formation, and  $\phi$  the dose (dpa).

The impact on the resistivity of both types of defects was similar: a prompt increase with the dose preceding a saturating tendency at higher dpa. After a high dose implantation, it was common to observe the crystalline–amorphous transition in implanted samples.<sup>23–25</sup> According to Fig. 5, the resistivity tends to saturate around 5–6 dpa, assuming a saturation of defect formation. This may explain why no amorphization of the structure was reported in TEM observations in the previous study on Ar-5dpa.<sup>14</sup>

The contribution level saturation for each defect type differed slightly, with  $\Delta\rho_{sat}^{300K}$  (PD)  $\sim 2.4 \times 10^{-5} \Omega\text{m}$  and  $\Delta\rho_{sat}^{300K}$  (Complex)  $\sim 1.8 \times 10^{-5} \Omega\text{m}$ . Therefore, the contribution of point-like defects seemed to be slightly larger in comparison to the contribution of complex defects on the resistivity. In addition, the effective cross section of damage was identical for both defects,  $\sigma = 0.75 \pm 0.1 \text{ dpa}^{-1}$ , suggesting a similar production process via displacement cascades. This means that both defect types were generated during the implantation process and did not result from possible evolution during *in situ* annealing. The  $\bar{n}_e$  (Fig. 2) remained constant between the meas. 1 and meas. 2, indicating that the complex defects were initially formed in the sample before any measurement/annealing.

This last investigation on cumulated implantation showed that a cumulative implantation process can be used as a tool to anticipate the influence of defects on the electrical properties of the sample and, thus, help on optimizing the experimental conditions.

#### IV. CONCLUSION

In conclusion, this study shows that the implantation of noble gas in degenerated ScN films allows the formation of two groups of defects named point- and complex-like defects. The complex-like defects were found to introduce deep acceptor levels in the bandgap. They also modified the electrical transport properties by acting as carriers' scattering centers and traps keeping the conduction mode of metallic-like behavior. In contrast, the point-like defects induced localized states close to the Fermi level leading to a change of the electrical conduction mode of the ScN films. Consequently, in the low temperature domain, the electrical conduction mechanism was dominated by the variable range hopping. The recovery of the point-like defects, which were observed by a simple temperature annealing, occurred as early as 400 K, yielding a recovery of the metallic-like behavior of the implanted films. In addition, the analysis of results showed, according to Mott's model, that the localization parameter was linked with the concentration of these point-like defects. In the case of the accumulation doses, the kinetics of both types of defects followed a direct impact model revealing that they formed directly within the cascade of

displacement. Finally, regardless of the nature of species implanted, the level of defects created (dpa) governed the changes in electrical transport properties after implantation.

#### ACKNOWLEDGMENTS

This work was supported by the French government program "Investissements d'Avenir" (EUR INTREE, Reference No. ANR-18-EURE-0010 and LABEX INTERACTIFS, Reference No. ANR-11-LABEX-0017-01). The authors also acknowledge funding from the Swedish Research Council (VR) under Project No. 2021-03826, the Knut and Alice Wallenberg Foundation through the Wallenberg Academy Fellows program (Grant No. KAW 2020.0196), the Swedish Government Strategic Research Area in Materials Science on Functional Materials at Linköping University (Faculty Grant SFO-Mat-LiU No. 2009 00971), and the Swedish Energy Agency under Project No. 46519-1.

#### AUTHOR DECLARATIONS

##### Conflict of Interest

The authors have no conflicts to disclose.

##### Author Contributions

**Razvan Burcea:** Conceptualization (equal); Data curation (lead); Formal analysis (equal); Investigation (equal); Methodology (lead); Validation (equal); Visualization (lead); Writing – original draft (lead); Writing – review & editing (equal). **Hugo Bouteiller:** Data curation (equal); Investigation (equal); Methodology (equal); Validation (equal); Writing – review & editing (equal). **Simon Hurand:** Formal analysis (equal); Investigation (equal); Methodology (equal); Validation (equal); Writing – review & editing (equal). **Per Eklund:** Conceptualization (supporting); Funding acquisition (equal); Validation (supporting); Writing – review & editing (supporting). **Jean-François Barbot:** Conceptualization (equal); Formal analysis (equal); Funding acquisition (equal); Investigation (equal); Supervision (lead); Validation (equal); Writing – original draft (equal); Writing – review & editing (equal). **Arnaud le Febvrier:** Conceptualization (equal); Investigation (equal); Supervision (equal); Validation (equal); Writing – review & editing (equal).

##### DATA AVAILABILITY

The data that support the findings of this study are available from the corresponding authors upon reasonable request.

##### REFERENCES

1. Biswas and B. Saha, *Phys. Rev. Mater.* **3**, 0202301 (2019).
2. D. Rao, A. I. K. Pillai, M. Garbrecht, and B. Saha, *Adv. Electron. Mater.* **9**, 2200975 (2023).
3. P. Eklund, S. Kerdsonpanya, and B. Alling, *J. Mater. Chem. C* **4**, 3905 (2016).
4. P. V. Burmistrova, J. Maassen, T. Favaloro, B. Saha, S. Salamat, Y. R. Koh, M. S. Lundstrom, A. Shakouri, and T. D. Sands, *J. Appl. Phys.* **113**, 153704 (2013).
5. S. Kerdsonpanya, N. Van Nong, N. Pryds, A. Zukauskaitė, J. Jensens, J. Birch, J. Lu, L. Hulman, G. Wingqvist, and P. Eklund, *Appl. Phys. Lett.* **99**, 232113 (2011).

26 March 2024 08:54:35

- <sup>6</sup>V. Rawat, Y. K. Koh, D. G. Cahill, and T. D. Sands, *J. Appl. Phys.* **105**, 024909 (2009).
- <sup>7</sup>N. Tureson, N. Van Nong, D. Fournier, N. Singh, S. Acharya, S. Schmidt, L. Belliard, A. Soni, A. le Febvrier, and P. Eklund, *J. Appl. Phys.* **122**, 025116 (2017).
- <sup>8</sup>B. Saha, J. A. Perez-Taborda, J. H. Bahk, Y. R. Koh, A. Shakouri, M. Martin-Gonzalez, and T. D. Sands, *Phys. Rev. B* **97**, 085301 (2018).
- <sup>9</sup>P. V. Burmistrova, D. N. Zakharov, T. Favaloro, A. Mohammed, E. A. Stach, A. Sakouri, and T. D. Sands, *J. Mater. Res.* **30**, 626–634 (2015).
- <sup>10</sup>S. Kerdsonpanya, O. Hellman, B. Sun, Y. K. Koh, J. Lu, N. Van Nong, S. I. Simak, B. Alling, and P. Eklund, *Phys. Rev. B* **96**, 195417 (2017).
- <sup>11</sup>S. Kerdsonpanya, B. Alling, and P. Eklund, *Phys. Rev. B* **86**, 195140 (2012).
- <sup>12</sup>N. Tureson, M. Marteau, T. Cabioch, N. Van Nong, J. Jensen, J. Lu, G. Greczynski, D. Fournier, N. Singh, A. Soni, L. Belliard, P. Eklund, and A. le Febvrier, *Phys. Rev. B* **98**, 205307 (2018).
- <sup>13</sup>D. Rao, O. Chowdhury, A. I. K. Pillai, G. K. Pradhan, S. Sahoo, J. P. Feser, M. Garbrecht, and B. Saha, *ACS Appl. Energy Mater.* **5**(6), 6847 (2022).
- <sup>14</sup>R. Burcea, J.-F. Barbot, P. O. Renault, D. Eyidi, T. Girardeau, M. Marteau, F. Giovannelli, A. Zenji, J.-M. Rampnoux, S. Dilhaire, P. Eklund, and A. le Febvrier, *ACS Appl. Energy Mater.* **5**, 11025 (2022).
- <sup>15</sup>A. le Febvrier, L. Landälv, T. Liersch, D. Sandmark, P. Sandström, and P. Eklund, *Vacuum* **187**, 110137 (2021).
- <sup>16</sup>J. F. Ziegler, M.-D. Ziegler, and J.-P. Biersack, *Nucl. Instrum. Methods Phys. Res., Sect. B* **268**, 1818–1823 (2010).
- <sup>17</sup>B. Saha, M. Garbrecht, J. A. Perez-Taborda, M. H. Fawey, Y. R. Koh, A. Shakouri, M. Martin-Gonzalez, L. Hultman, and T. D. Sands, *Appl. Phys. Lett.* **110**, 252104 (2017).
- <sup>18</sup>P. Bougiatioti, O. Manos, C. Klewe, D. Meier, N. Teichert, J.-M. Schmalhorst, T. Kushel, and G. Reiss, *J. Appl. Phys.* **122**, 225101 (2017).
- <sup>19</sup>N. F. Mott and E. A. Davis, *Electronic Process in Non-Crystalline Materials* (Oxford University Press, 1971).
- <sup>20</sup>L. Pizzagalli, A. Charaf-Eddin, and S. Brochard, *Comput. Mater. Sci.* **95**, 149 (2014).
- <sup>21</sup>V. Raineri, M. Saggio, and E. Rimini, *J. Mater. Res.* **15**, 1449 (2000).
- <sup>22</sup>J.-F. Gibbons, *Proc. IEEE* **60**, 1062 (1972).
- <sup>23</sup>D.-K. Sadana, *Nucl. Instrum. Methods Phys. Res., Sect. B* **7–8**, 375 (1985).
- <sup>24</sup>L. Pelaz, L. A. Marqués, and J. Barbolla, *J. Appl. Phys.* **96**, 5947 (2004).
- <sup>25</sup>S. Leclerc, M.-F. Beaufort, J.-F. Barbot, and A. Declémy, *Europhys. Lett.* **98**, 46001 (2012).